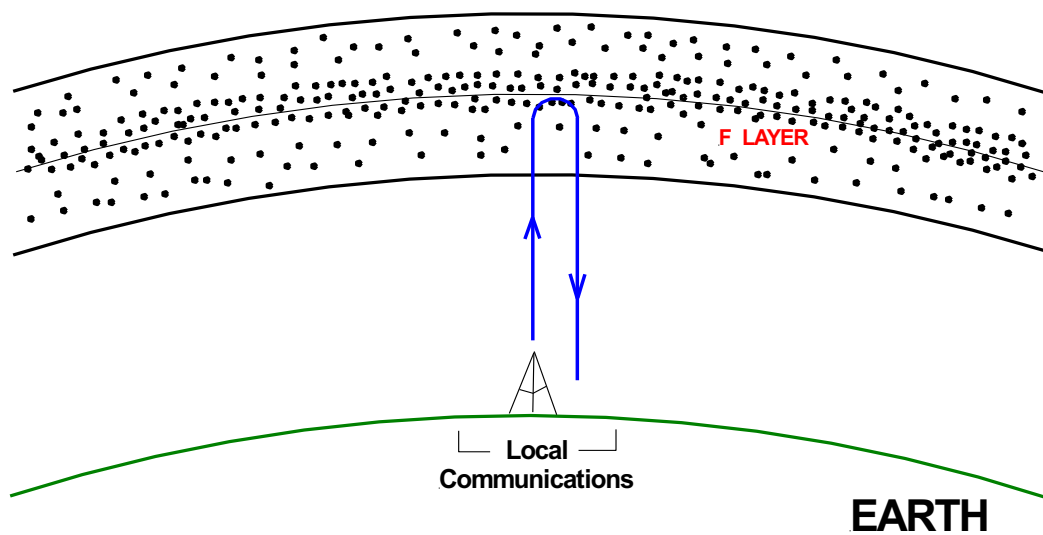


Chapter 16

Ionosphere Critical Frequency



16 Critical Frequency

Critical frequency f_c is the highest frequency radio signal that can be transmitted straight up and be reflected by the ionosphere back to Earth (Figure 1). Higher frequency radio signals pass through the ionosphere and are lost to outer space.

Critical frequency is very important in over the horizon HF radio communications. It determines the maximum frequency that can be used in communicating between two radio stations.

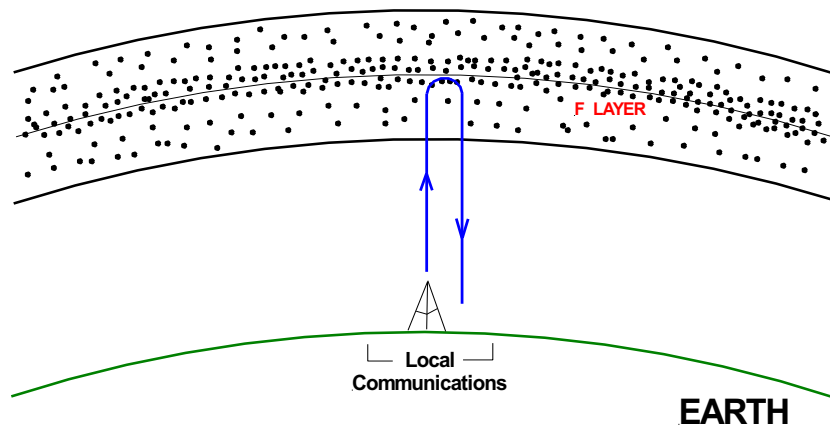


Figure 1 Critical Frequency (source: author)

Regions E, F1, and F2 each have their own critical frequency, specifically f_{cE} , f_{cF1} , and f_{cF2} .

16.1 Plasma Frequency

Plasma frequency is approximately equal to the ionosphere's resonant frequency.

Free electrons and ions are not stationary. Instead they are in constant motion. In addition, electrostatic forces between positive ions and negative electrons causes an electron to oscillate back and forth in simple harmonic motion around an ion. Ions are massive compared to tiny electrons. Consequently, it is the tiny electron that experiences harmonic motion around a heavy fixed ion. The frequency of oscillation, called the plasma frequency, is

$$\omega^2 = \frac{N(h) \cdot e^2}{\epsilon_0 m}$$

where

ω = angular frequency (radians per second)

$N(h)$ = electron density per cm^3 at an altitude h above Earth's surface

e = electrical charge on an electron

ϵ_0 = permittivity of free space

m = mass of an electron

Converting from radians per second ω to hertz f where

$$f = \frac{\omega}{2\pi}$$

and substituting in the values for the constants e , ϵ_0 , and m , plus changing to MHz gives

$$\text{Plasma Freq} = f \approx 9(10^{-3})\sqrt{N(h)} \text{ MHz}$$

16.2 Region E, F1, and F2 Critical Frequencies

The critical frequency for a particular region (E, F1, or F2) is defined as the highest plasma frequency in that particular region of the ionosphere. As we saw earlier, critical frequency is also the highest frequency signal that can be transmitted straight up and reflected back to Earth from a particular ionospheric region. Each region has its own critical frequency.

Critical frequency occurs at the altitude h where the electron density $N(h)$ is maximum. For the F2 region in Figure 2, the maximum density occurs at an altitude of 180 miles (~290 km) where

$$\text{Electron Density } N(180 \text{ mi}) = 10^6 \text{ electron per cubic centimeter}$$

and the critical frequency is

$$f_{cF2} = 9(10^{-3})\sqrt{N_{F2}(h)} = 9 \text{ MHz}$$

If the maximum electron densities for the E, F1, and F2 regions are respectively

- $N_E = 2 \times 10^5$,
- $N_{F1} = 5 \times 10^5$, and
- $N_{F2} = 1 \times 10^6$

then the critical frequencies are

- $f_c E = 4 \text{ MHz}$
- $f_c F1 = 6.6 \text{ MHz}$, and
- $f_c F2 = 9 \text{ MHz}$

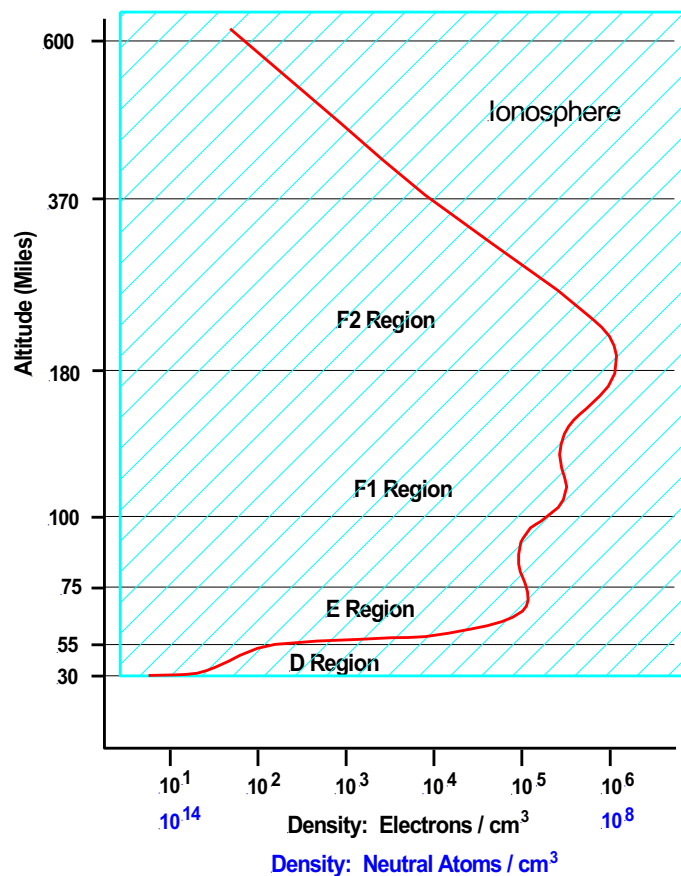


Figure 2 Ionospheric electron density profile (source: author)

A vertical 4 MHz signal will be reflected back to Earth by the E region. A 6.6 MHz signal will pass through the E region and be reflected back to Earth by F1. A 9 MHz signal will pass through both E and F1 and reflect back to Earth from the F2 region. A vertical 10 MHz signal will pass through the ionosphere and be lost to outer space.

16.3 Ionospheric Sounding

Ground based sounders, known as ionosondes Figure 3, have been used since the early days of radio to probe the ionosphere. They have provided the bulk of our current information on ionospheric structure.



Figure 3 Ionosonde controller and data processor (source: Electronics Notes)

16.3.1 Ionosonde systems

A typical ionosonde system is shown in Figure 4. An ionosonde transmits a pulsed signal straight up into the atmosphere and receives an echo, or reflection, of the signal back from the ionosphere. The condition of the echoed signal, whether it is reflected or not, the width and frequency of the reflected pulse, and the time between transmission and reception provides information on the current condition of the ionosphere. The time between transmission and reception of a pulse indicates the height at which the signal was reflected.

An ionosonde utilizes a sweep frequency transmitter. The transmitter, driven by the ionosonde processor, sends a long series of pulses, each at a slightly different frequency over a frequency range of typically 0.5 to 25 MHz. A radio signal transmitted vertically will penetrate the ionosphere until it reaches an altitude at which its frequency equals the ionosphere plasma frequency. At that point it is reflected back to ground.

The ionosonde processor tunes the receiver to the frequency of the transmitted signal. The echo of the transmitted pulse is received by the receiver and sent to the processor.

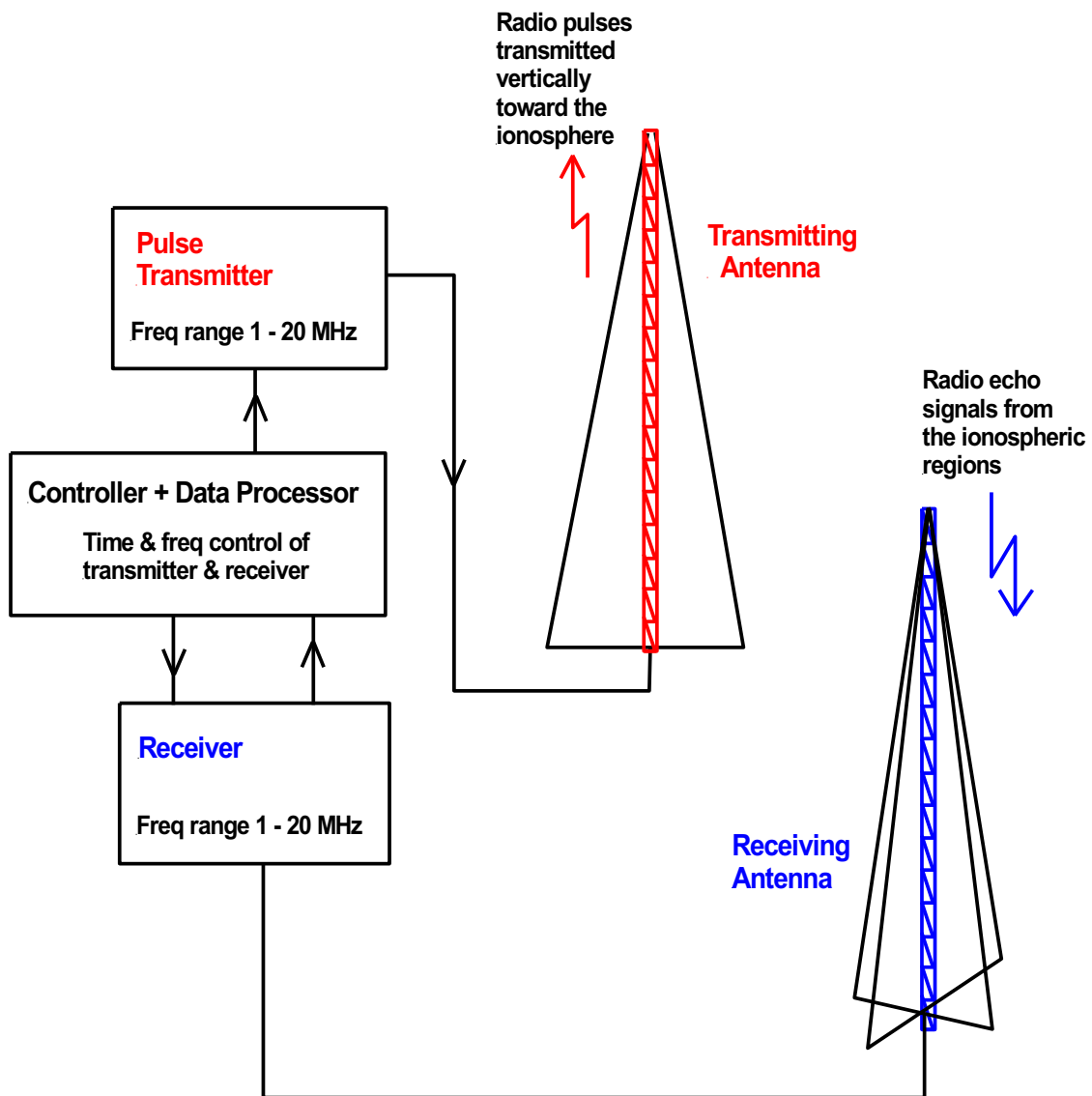


Figure 4 Ionosonde system diagram (source: spaceacademy.net.au)

The processor converts the received echo into a graphical display of echo time delay verses frequency. The display is known as an ionogram. On the ionogram, echo delay is converted to altitude of the reflection point using the equation

$$\text{Altitude km} = (1/2) c T$$

where

c = speed of light

T = time delay between transmission and reception of a pulse.

The factor $1/2$ appears in the equation because T is the total round trip time to the reflection point and back again. The time from the transmitter to the reflection point is one half that ($1/2 T$).

For example, in the ionogram shown in Figure 5 a signal reflected at a frequency of $\sim 3\text{MHz}$ indicating the presence of an E region. A 4.2MHz signal passed through the E region and is reflected by the F1 layer identified by the longer time between transmission and reception of the pulse. A 5.1MHz signal passed through both E and F1 before being reflected in the F2 region, represented by a still longer delay. In this example a 7MHz pulse passes through all 3 layers without being reflected and is lost to outer space.

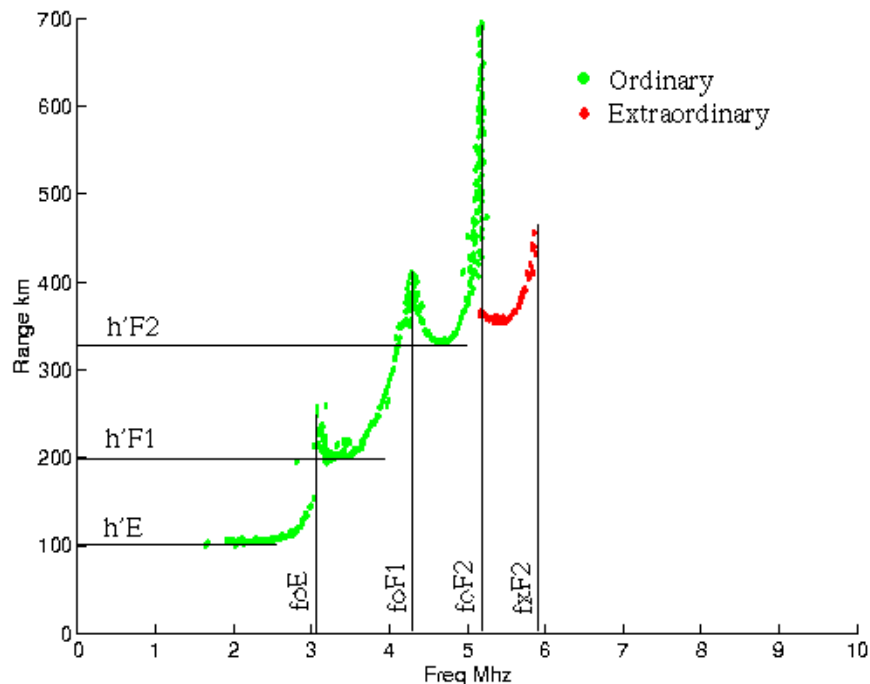


Figure 5 An ionogram graphical display (source: ukssddc.ac.uk)

16.3.2 Ordinary and Extra Ordinary Modes

Earth's geomagnetic field causes a HF radio signal to split into two different signals as it enters the ionosphere. The two signals each have a slightly different mode of propagation through the ionosphere (slightly different indices of refraction resulting in slightly different velocities, reflection heights, and direction of travel). One propagation mode is termed the ordinary or o-mode. The other is called the extraordinary mode, or x-mode. Consequently, each ionogram consists of two traces, one corresponding to the o-mode (red trace) and the other to the x-mode (green trace) in Figure 6.

At a frequency of 4 MHz in Figure 6 the o-mode signal reflects at a lower altitude than the x-mode (230 vs 250 km). At a frequency of 7 MHz the situation is reversed. At 7 MHz the x-mode reflects at 280 km while the o-mode reflects at 340 km. Because of the higher reflection altitude, the 7 MHz hop distance for the o-mode signal is longer than the x-mode signal.

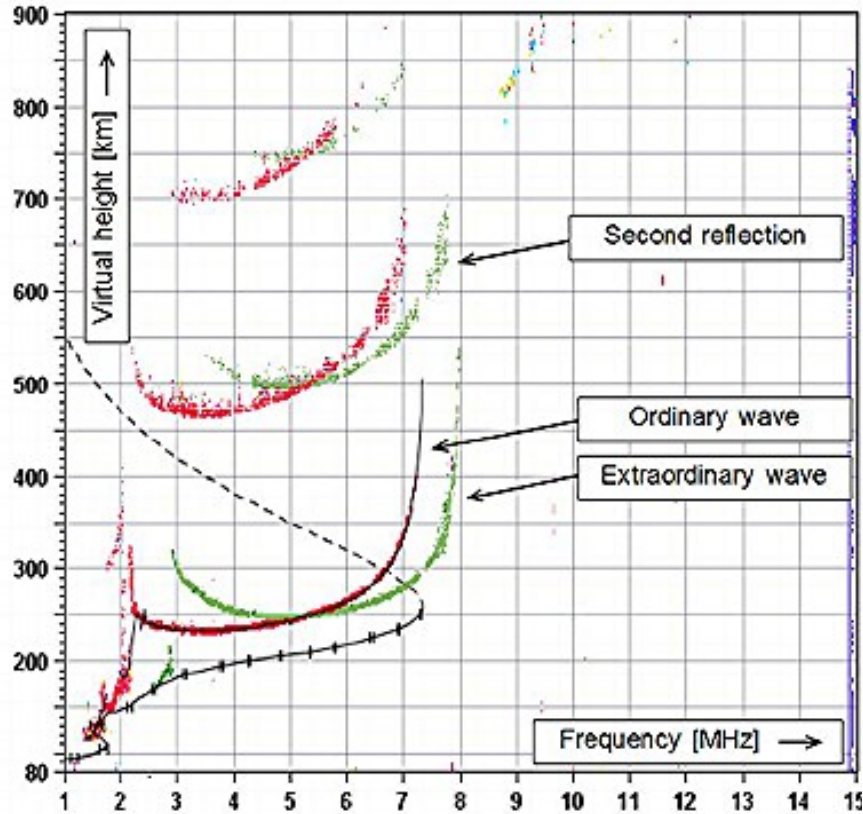


Figure 6 Ionogram showing both ordinary and extra ordinary modes (source: ResearchGate)

16.3.3 Reading an Ionogram

By convention the o-mode trace is used in determining the critical frequencies and maximum electron densities at the points of reflection. The o-mode (f_o) critical frequency f_oF2 is

$$f_oF2 = 9(10^{-3})\sqrt{N_{max}}$$

where N_{max} is the maximum electron density and f_oF2 is read from the ionogram. From this information the maximum electron density N_{max} in the F2 region can be calculated from

$$N_{max} = \left[\frac{f_oF2}{9(10^{-3})} \right]^2$$

In Figure 7, f_oF2 is the o-mode F2 critical frequency and f_xF2 is the x-mode F2 critical frequency. $h'F2$ is the height (altitude) of the F2 maximum electron density.

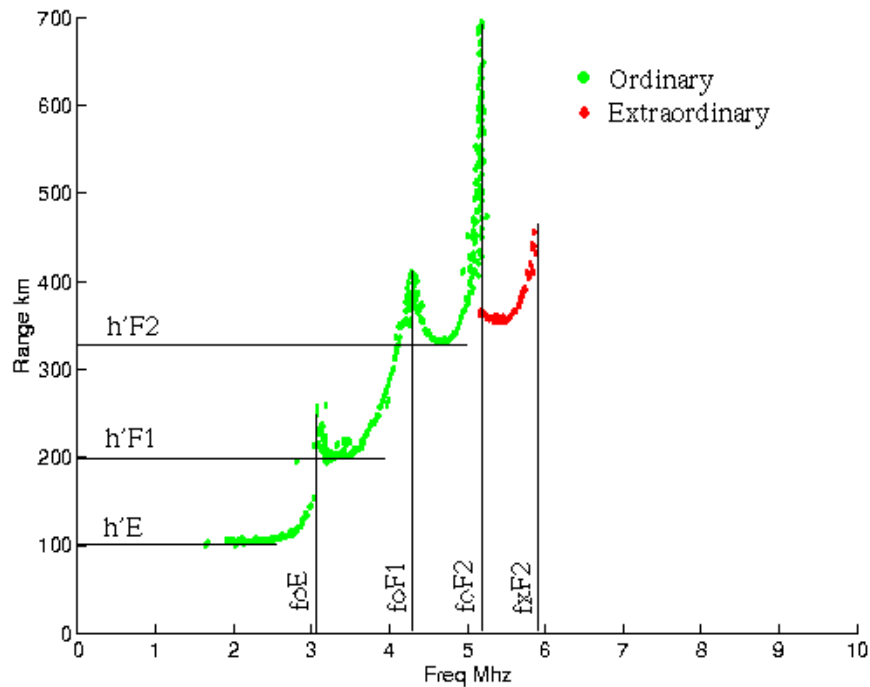


Figure 7 An ionogram graphical display (source: ukssddc.ac.uk)

The transmitted signal from the ionosonde is assumed to travel at the speed of light c . However, this is not really the case. The speed of the transmitted signal traveling through the ionosphere is actually less than c . In addition, its speed varies as the electron density of the ionosphere changes with altitude. The speed decreases significantly as the sweep frequency of the transmitter approach a critical frequency point, considerably increasing the reflection time T at that point. On an ionogram, the increase in T appears as a spike in the height at which critical frequency reflection occurs. This is an artifact. The reflection heights are actually $h'E$, $h'F1$, and $h'F2$ as shown in Figure 7. However, the spikes make it easy to identify the critical frequency points.

16.3.4 Types of Ionosondes

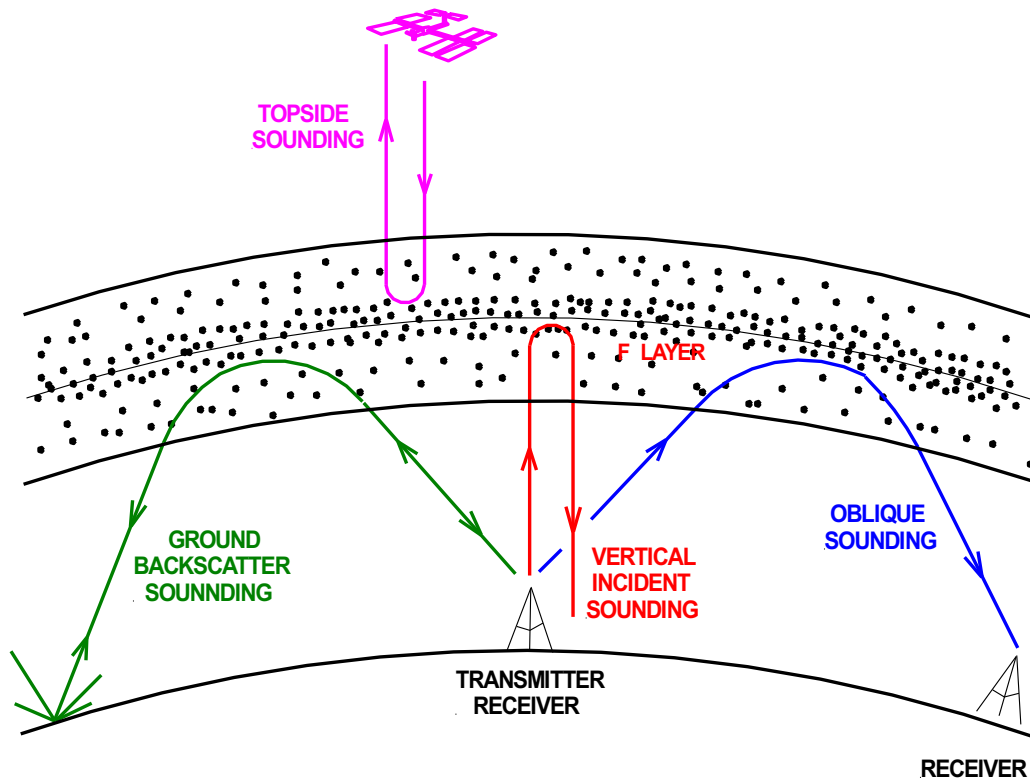


Figure 8 Types of Ionosondes (source: author)

Several types of ionosonde sounders (also known as HF radar) are currently in use. These are illustrated in Figure 8. They include:

- Vertical incident sounders (VIS),
- Oblique sounders,
- Direct and ground backscatter radar, and
- Topside sounding using Earth satellites.

16.3.4.1 Vertical Incident Sounders (VIS)

Vertical incident sounding (VIS) transmits a sweep frequency HF signal vertically into the atmosphere and receives the echoes, or reflections, from the ionosphere on a co-located receiver as illustrated in Figures 4, 8 and 9. Vertical incident sounding is the earliest method used for investigating the ionosphere. Over the years it has provided a very complete picture of ionospheric structure. It remains the primary method for determining current ionospheric conditions in the E, F1, and F2 regions. However, determining current D region conditions is a problem. Because of D region signal absorption, special methods are needed to determine electron densities in this region.

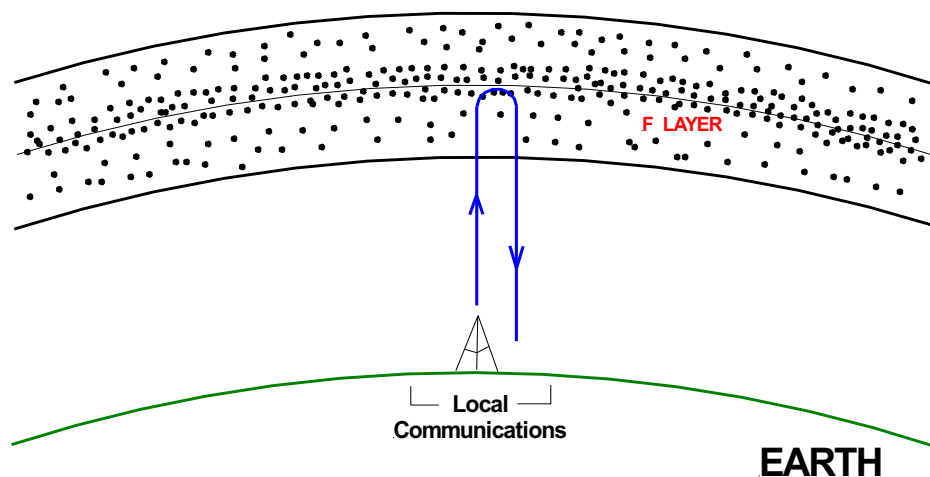


Figure 9 Vertical Incident Sounding (source: author)

Much of the current ionospheric nomenclature has evolved from the early VIS investigations. Typical VIS specifications include:

Frequency	0.5 to 25 MHz
Power	300 W to 10 KW
Sweep Cycle	30 sec – 5 min.
Pulse Rate	50 per sec
Pulse Width	30 microsec

16.3.4.2 Oblique Sounding

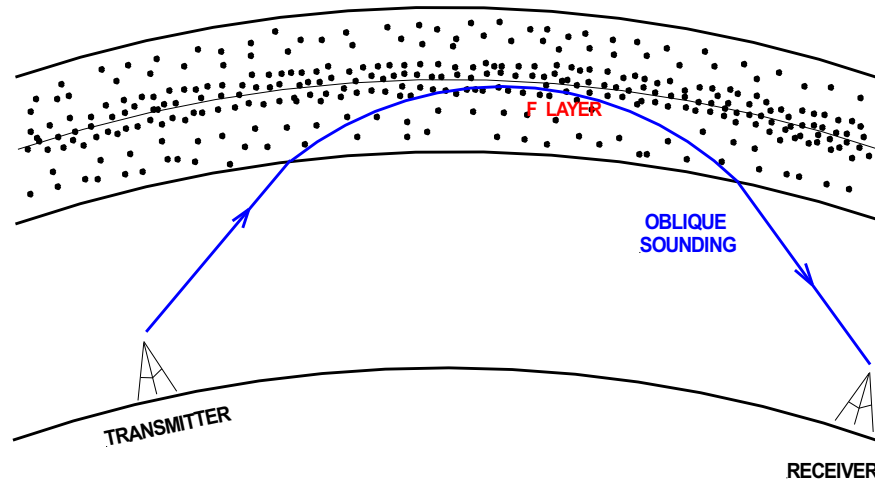


Figure 10 Oblique Sounding (source: author)

Oblique sounding monitors propagation conditions on an HF communications circuit between two locations as illustrated in Figures 8 and 10. This is done by transmitting pulses of radio energy obliquely through the ionosphere from a sweep frequency transmitter to a distant receiver. The transmitter and receiver must be synchronized in order to produce an oblique ionogram. Oblique sounding is very important for real time radio frequency management. It is used to determine which frequencies and propagation modes are available over a particular communications circuit at the time of operation. It is also very important for testing propagation predictions and validating ionospheric models. Monitoring HF broadcast transmitters such as WWV, WWVH, and W1AW transmissions is a form of passive oblique sounding. The receiving station can determine current HF conditions by monitoring the strength and stability of the broadcast station.

16.3.4.3 Backscatter HF Radar

Signals transmitted into the ionosphere are often scattered by ionospheric irregularities. Some of the scattered signal is received back at the transmitting site as illustrated in Figures 8 and 11. Two types of backscatter HF radar systems are in use. They are:

- Direct Backscatter Radar
- Ground Backscatter Radar

Both types are used to study ionospheric irregularities. Backscatter HF Radars are typically expensive complex systems frequently utilizing large arrays of up to 16 log-periodic antennas.

Interpretation of backscatter data is often complex.

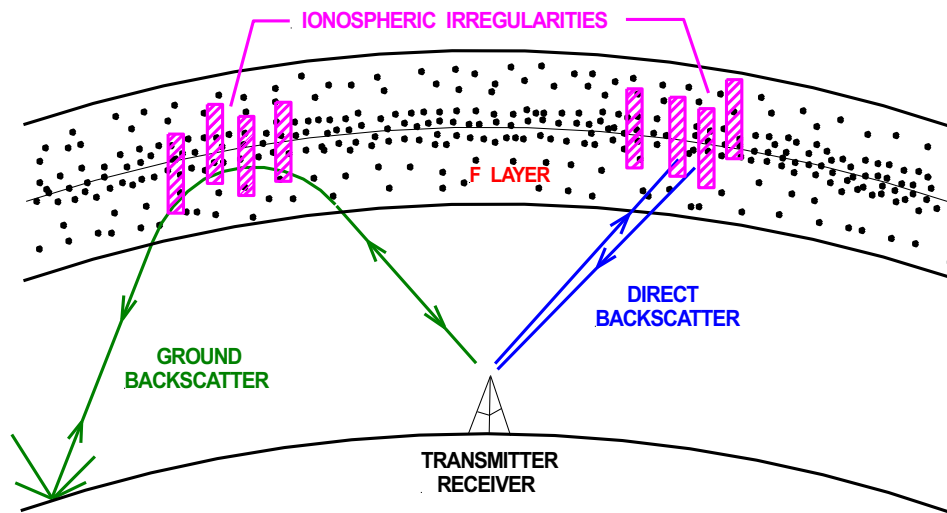


Figure 11 Backscatter HF Radar (source: author)

Direct backscatter HF radar are systems designed to make use of the backscatter phenomena to study ionospheric irregularities by analyzing the received backscattered signal. Networks of direct backscatter systems are used to study the high latitude ionosphere. All of the north polar region is covered and part of the south polar region.

All signals that are transmitted into the atmosphere and refracted back to Earth by the ionosphere, scatter when they hit the ground. A small amount of scattered energy travels back through the ionosphere to the transmitting site. The returning signal (ground echo) is often distorted by ionospheric irregularities. These irregularities are studied by analyzing the distorted ground echo. Ground backscatter signals are orders of magnitude weaker than direct backscatter signals.

16.3.4.4 Top Side Sounding

Top side sounding utilizes Earth satellites to probe the upper part of the ionosphere as illustrated in Figure 12. Ground based ionosondes can only “see” the bottom of the ionosphere, up to the F2 maximum ionization level, by transmitting at frequencies at and below the F2 critical frequency f_cF2 . Higher frequency vertical signals pass through the ionosphere without being reflected back to Earth, and thus provide no information. Top side sounding from an Earth satellite is very similar to ground based VIS except it probes down into the ionosphere from above. The F2 maximum ionization level is the furthest that a top side sounder can see down into the ionosphere, again by transmitting at frequencies at and below the F2 critical frequency f_cF2 . Transmitting at a higher frequency will cause the signal to pass through the ionosphere to the Earth instead of being reflected back to the satellite. Consequently, top side sounders explore the ionosphere from the F2 maximum ionization level to an altitudes of 1,000 km or more.

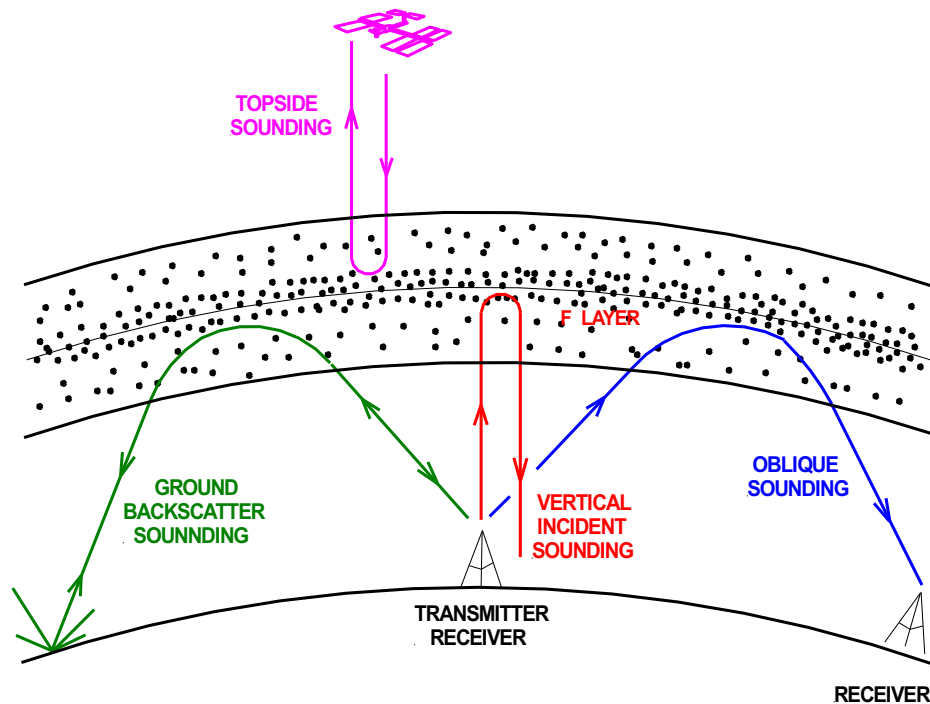


Figure 12 Top Side Sounding (source: author)

16.4 Variations In Critical Frequencies

Critical Frequencies vary:

- Over the 11 year solar cycle,
- Seasonally, and
- Throughout the day (diurnal).

16.4.1 Variations In Critical Frequencies Over An 11 Year Solar Cycle

Sunspots, as we know, are black irregularly shaped blemishes on the Sun's surface (Figure 13). [See the chapter "The Active Sun" for an in depth discussion of sunspots.] Sunspots appear, increase in number, and then gradually disappear over roughly an 11 year cycle. A series of sunspot cycles, more generally referred to as solar cycles, is shown in Figure 14. Solar cycle numbers 23 and 24 are shown in the figure along with a prediction for Solar Cycle 25.



Figure 13 Sunspot groups (credit: NASA Goddard Space Flight Center)

A solar cycle arbitrarily begins at sunspot minimum when few if any sunspots are visible on the solar disk. When a sunspot does appear, it lasts several days and then disappears. Some sunspots may last for several weeks.

For Solar Cycle 24 sunspot minimum occurred in 2009 with no sunspots visible on the Sun (sunspot number = 0). Over the next few years the number of sunspots slowly increased peaking at sunspot maximum in 2014 with around 110 sunspots visible at any given time. This was a relatively small number of sunspots for a sunspot maximum. Solar cycle 23 had nearly 170 sunspots at sunspot maximum. The number of sunspots for Solar Cycle 24 gradually decreased from its peak in 2014 to the next sunspot minimum in 2019 marking the end of Solar Cycle 24. Figure 15 shows two views of the Sun, one during solar minimum (on the left) with no sunspots visible and the other during solar maximum with a large number of visible sunspots.

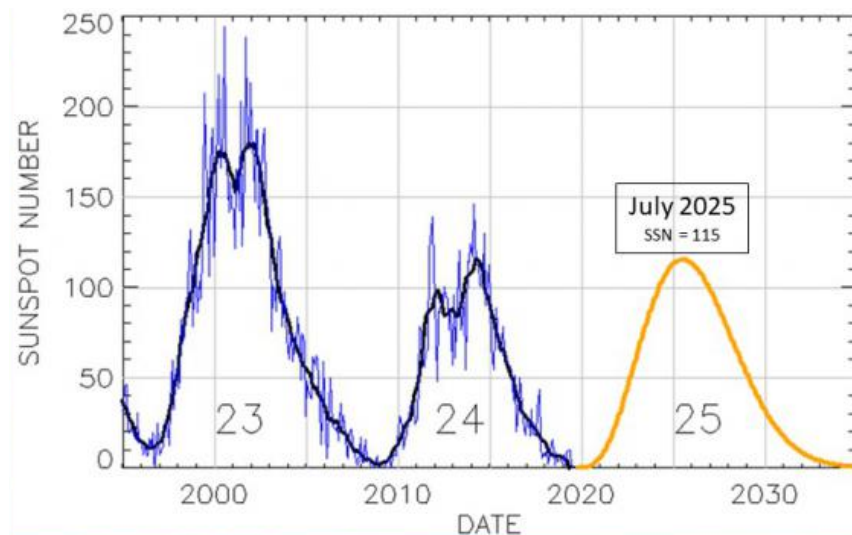


Figure 14 Projections for Solar Cycle 25 (credit: NOAA Space Weather Prediction Center)

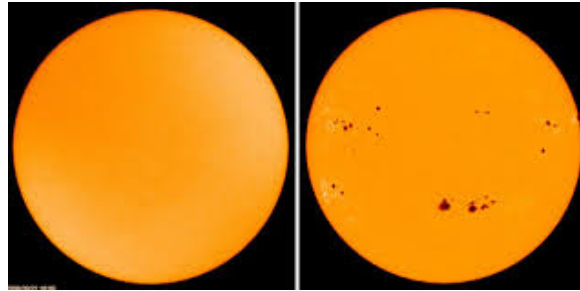


Figure 15 Sun at solar minimum and maximum (credit: springer.com)

As discussed in earlier chapters, the solar cycle is a direct consequence of the Sun's turbulent magnetic field. The magnetic field is produced by vertically circulating electrical currents in the Sun's convection zone, and stressed by the Sun's differential rotational rate. The convection zone lies just below the photosphere as illustrated in Figure 16. The photosphere is what we perceive as the Sun's surface. A circulating electrical current produces a magnetic field, in this case the Sun's magnetic field. In Figure 16 the circulating currents are represented by curved arrows in the convection zone.

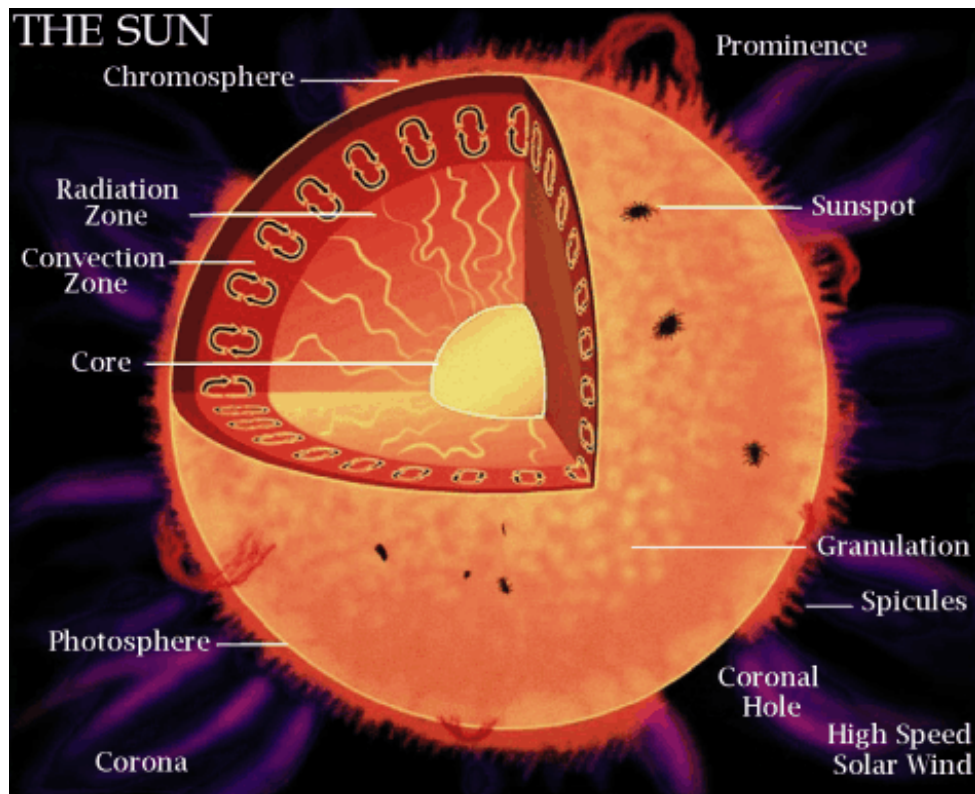


Figure 16 The Sun (credit: NASA).

The Sun of course is not solid. It is a huge rotating ball of gas. Furthermore, the gas does not rotate at the same rate. The Sun's equator rotates in 24.5 days while the poles rotate in 34 days. Variations in the Sun's rotational rate with latitude is referred to as differential rotation.

The fact that the Sun's magnetic field is created near its surface, instead of deep within the Sun, coupled with the Sun's differential rotation, causes the Sun's magnetic field to become badly twisted and distorted.

At sunspot minimum the Sun's magnetic field, shown in Figure 17a, is a "quiet" north – south bipolar field similar to that of Earth's magnetic field. The strength of Earth's magnetic field is around 0.2 gauss. At sunspot minimum the strength of the Sun's magnetic field is about 1.0 gauss. The Sun's quiet magnetic field is not that much different from Earth's magnetic field. Sunspot minimum for Solar Cycle 24 occurred in 2008 (Figure 18)

Over the next 3 years or so the Sun's differential rotation slowly drags and winds the magnetic field around the Sun as illustrated in Figure 17b. This is known as the ascending phase of the solar cycle. For Solar Cycle 24 the ascending phase occurred from 2009 to around 2012.

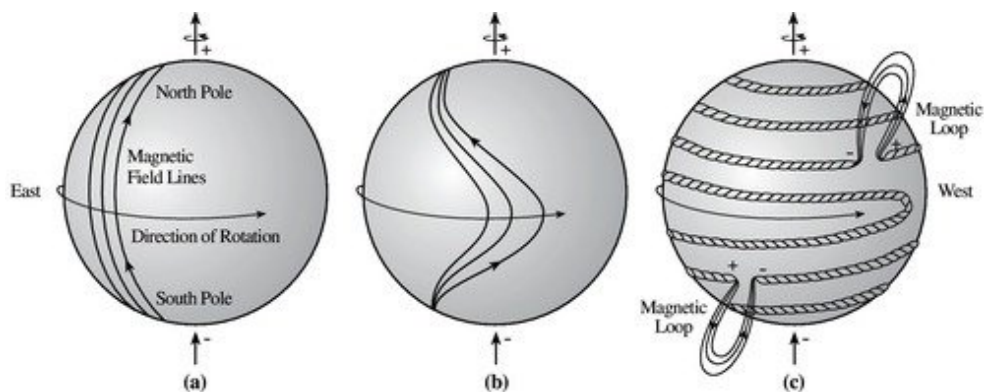


Figure 17 Magnetic field lines become wrapped and twisted around the Sun
(credit: NASA's Cosmos – ase.tufts.edu)

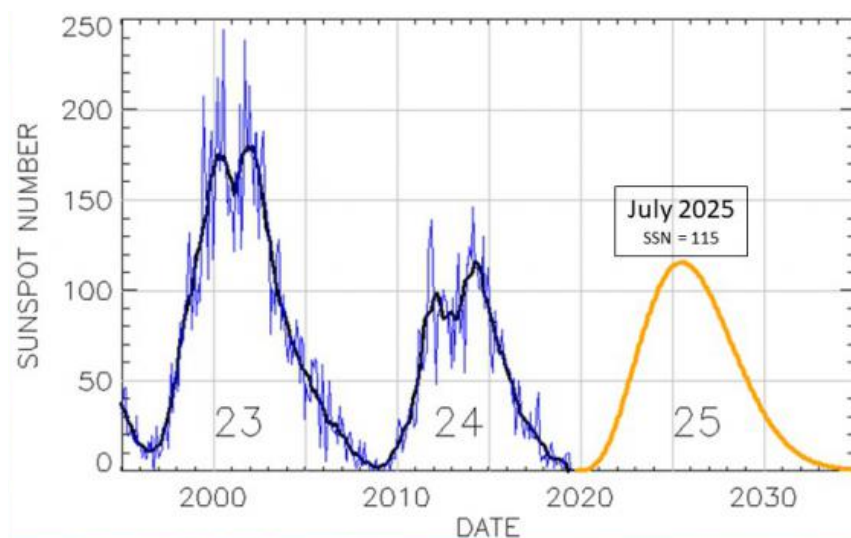
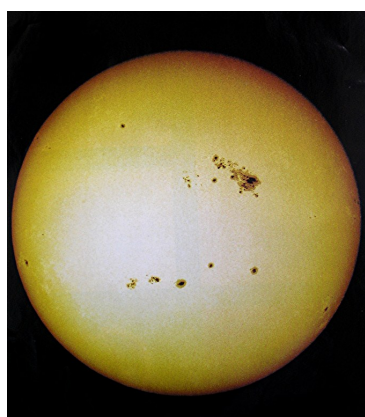
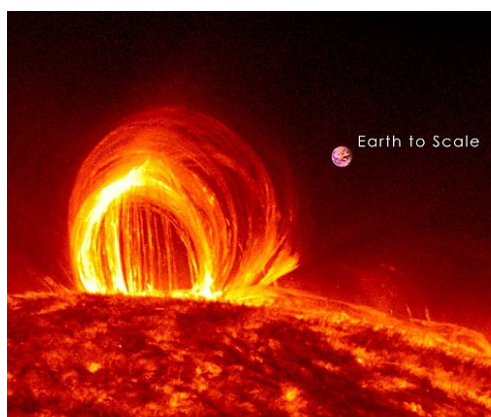


Figure 18 Solar Cycles 23 and 24 (credit: NOAA Space Weather Prediction Center)

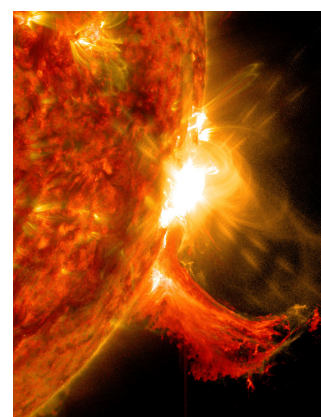
Differential rotation winds the magnetic field around the Sun in tighter ever increasing number of turns (Figure 17c). In addition, convection zone turbulence twists the magnetic field lines into ropes some of which become knotted. This is not a sustainable process. Something has to break, and it does! Continued winding, twisting, and knotting creates tremendous stress in the magnetic field driving field intensities to well over 3,000 gauss. The enormous stress eventually causes the field to rupture in many places across the Sun. As it does so sunspots, high arching coronal loops, and solar flares erupt from the Sun (Figure 19). The number of sunspots visible on the Sun reaches a maximum during this very turbulent period. This is solar maximum. Solar maximum for Solar Cycle 24 occurred from 2011 to 2015.



Sunspots



Coronal Loop



Solar Flare

Figure 19 Sun during solar maximum (source: NASA Goddard Space Flight Center)

Rupturing of the magnetic field causes it to disintegrate. As it disintegrates, the magnetic field unwinds, solar activity subsides, and sunspots gradually disappear. This is the declining phase of the solar cycle which for Solar Cycle 24 occurred from 2015 to 2019. In 2019 the number of visible sunspots reached zero defining the next solar minimum and the end of Solar Cycle 24.

Sunspots, like the one shown in Figure 20, occur at locations on the Sun where strong magnetic fields erupt through the photosphere (the photosphere is the yellow regions in Figure 20). The magnetic fields suppress the upward flow of hot plasma from deep in the convection zone. Starved of hot plasma, a sunspot is cooler than the surrounding photosphere which gives a sunspot its black appearance.

Associated with sunspots are hot bright irregularly shaped areas called plages (white regions in Figure 21). Plages are important because they emit copious amounts of EUV radiation responsible for ionizing Earth's upper atmosphere. Plages are formed in the chromosphere by intense magnetic fields radiating out from the photosphere. They occur in active sunspot regions of the Sun and usually form several days prior to sunspots in the area. In addition, plages typically last long periods of time, longer than their associated sunspots.

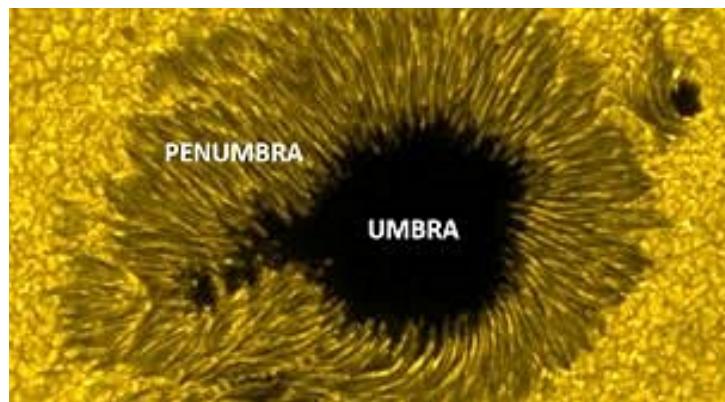


Figure 20 A closer look at sunspots (credit: spaceweatherlive.com)

While there is a strong correlation between sunspots and long distance radio communications, it turns out that sunspots have little to do with HF propagation. Sunspots are far too low in temperature to generate the EUV radiation needed to ionize Earth's upper atmosphere. The required EUV radiation is primarily produced by plages. The problem is that plages can not be seen (without special equipment) in the intense light emanating from the photosphere because the photosphere is too bright. But sunspots can easily be seen as readily apparent in Figure 19. Thus sunspots become markers for plages. A large number of sunspots means a large number of plages, high EUV levels, strong ionization of the Earth's ionosphere, and good HF radio communications. When they are present, the extreme heat of coronal loops also emit copious amounts of EUV radiation.

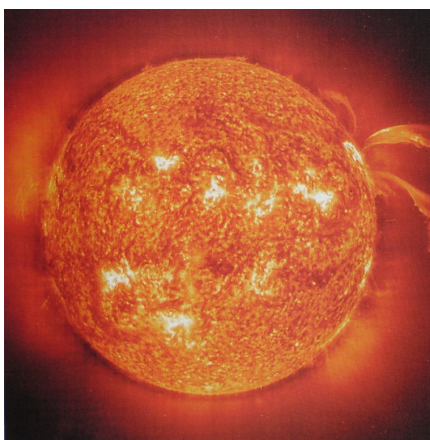


Figure 21 Sun's chromosphere shown in H alpha (H_{α}) light (credit: universitytoday.com)

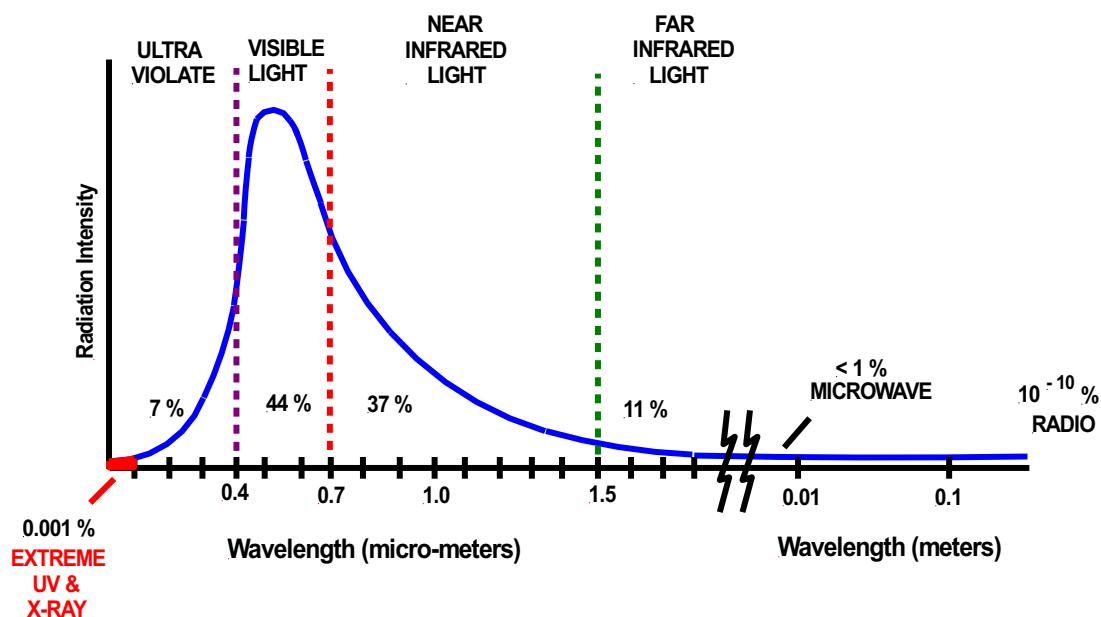


Figure 22 Sun's energy output (credit: author)

The EUV radiation responsible for ionizing Earth's upper atmosphere accounts for only 0.001% of the Sun's total energy output as illustrated in Figure 22. While the Sun's output remains incredibly stable over thousands of years, the Sun's EUV energy output is not stable at all! EUV energy varies considerably over the 11 year solar cycle. Consequently, the level of ionization in Earth's upper atmosphere also varies over the same time period. EUV energy output is greatest during solar

maximum when there are large numbers of sunspots, and consequently large numbers of EUV emitting plages. EUV output is lowest during solar minimum when there are few if any sunspots and only a few small randomly scattered plages.

The E, F1, and F2 critical frequencies all vary with the solar cycle as shown in Figure 23. This is to be expected. An increase in solar activity produces an increase in EUV radiation responsible for ionizing Earth's upper atmosphere.

The red trace in Figure 23 is the smoothed sunspot number (ssn) for the years 1988 through 2015. The smoothed sunspot number is the number of sunspots observed averaged over a 13 month period (refer to the "Short Article Sunspot Numbers" on the website www.skywave-radio.org for more details). The vertical scale on the right is the smoothed sunspot number. The scale on the left is critical frequency in MHz. The graph shows three solar cycles. The solar cycles shown on the right and left are partial solar cycles while the complete Solar cycle 23 is shown in the middle. Solar cycle 23 began as a minimum in late 1996 with sunspot numbers around 10 or so. Sunspot maximum occurred in mid 2000 and again in 2002 before declining to the next solar minimum in 2009.

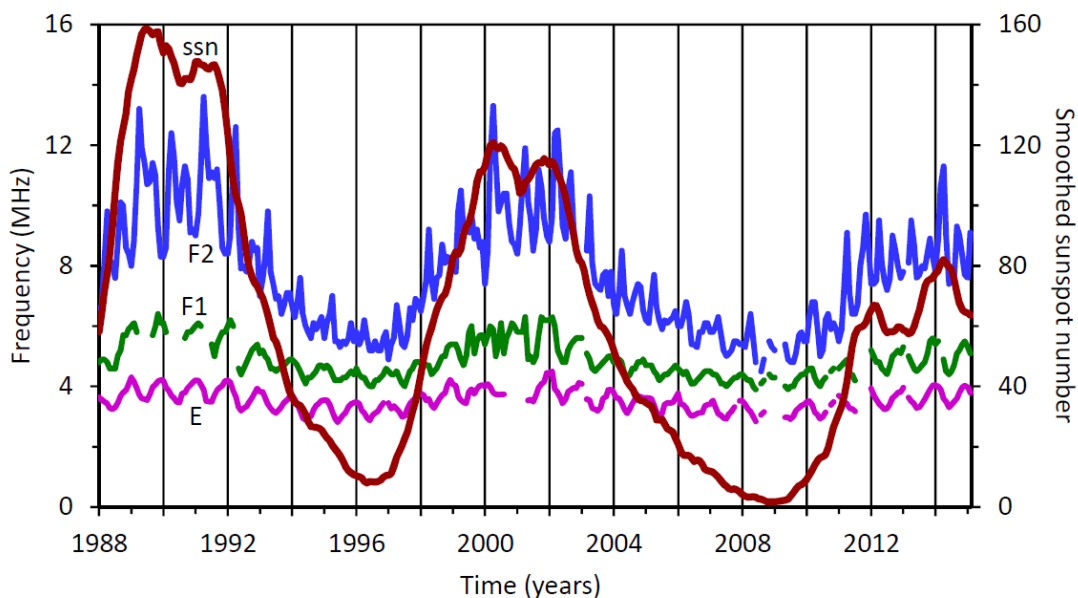


Figure 23 Variations of critical frequencies with the solar cycle (source: sws.bom.gov.au)

As can be seen in Figure 23, the solar cycle has the greatest effect on F2 critical frequencies. The highest F2 critical frequencies occur during solar maximums with critical frequencies typically ranging from 8 to 14 MHz. At solar minimum the typical F2 critical frequency range is 5 to 6 MHz. The highest F1 and E critical frequencies also occur during solar maximum. However, the solar cycle has less of an effect on F1 and E critical frequencies with the E region critical frequency being affected the least.

In general, solar EUV radiation changes by a factor of 10 over the course of an 11 year solar cycle as illustrated in Figure 24. In this figure the vertical axis is the percent change in EUV radiation from solar maximum to solar minimum. The horizontal axis is EUV wavelength. The graph shows the percent difference between solar maximum and minimum EUV radiation is greatest for high energy short wavelength EUV radiation. This accounts for the solar cycle having a greater effect on the F2 region of the ionosphere than on the E region. The F2 region is formed by high energy EUV radiation in the range from 20 to 90 nm ionizing individual oxygen atoms forming O^+ ions. This is the range of EUV radiation most effected by the solar cycle. In contrast, the E region is formed by lower energy EUV radiation in the range from 80 to 103 nm that ionizes molecular oxygen O_2 to form O_2^+ ions. In addition, lower recombination rates in the F2 region, coupled with electrons and ions drifting from the F1 into the F2 region, accentuates the F2 region variation with the solar cycle.

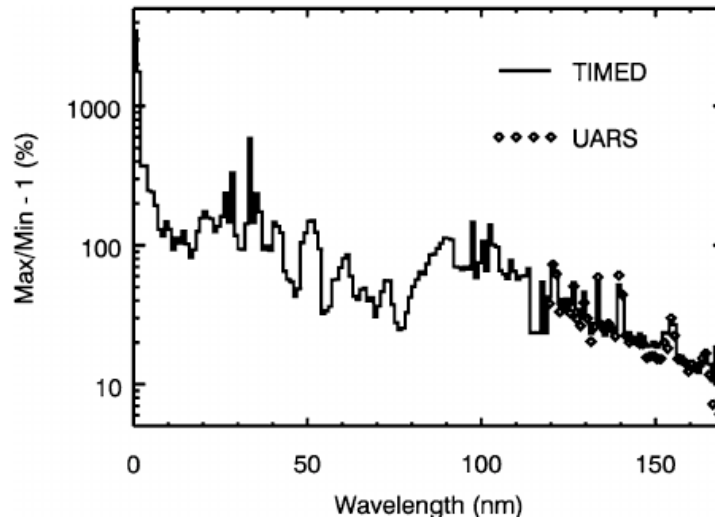


Figure 24 Solar cycle variation in EUV vs wavelength (source: ResearchGate)

As described earlier, the critical frequency for a particular ionospheric region is

$$f_c = 9(10^{-3})\sqrt{N(h)}$$

where $N(h)$ is the electron density at a given altitude h above Earth's surface. By making the appropriate substitutions the critical frequency equation can be expressed in terms of the number of sunspots (R) visible on the solar disk and the zenith angle χ at a particular latitude and time of day on Earth.

Critical frequencies for the Chapman like E and F1 regions depend on the number of sunspots present R and the zenith angle χ according to the equations

$$f_c E = 3.3[(1 + 0.008R)\cos \chi]^{1/4} \text{ MHz}$$

$$f_c F1 = 4.25[(1 + 0.015R)\cos \chi]^{1/4} \text{ MHz}$$

The F2 region critical frequency also depends on the sunspot number R, but not on the zenith angle. The equation for the F2 critical frequency is

$$f_c F2 \propto [1 + 0.02R]^{1/4} \text{ MHz}$$

Dependence on zenith angle is an important characteristic of Chapman layers such as the E and F1 regions. However, characteristics of the F2 region are much different from that of a Chapman layer. Consequently, zenith angle does not appear in the F2 critical frequency equation.

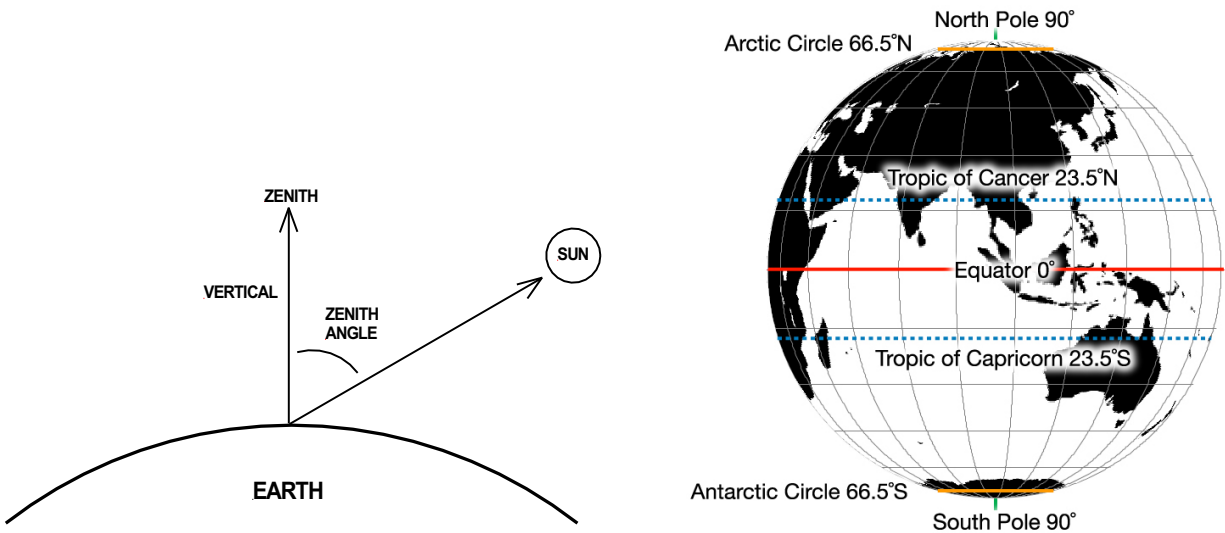


Figure 25 Zenith angle defined (source: author)

For clarification, zenith angle, illustrated in Figure 25, is the angle of the Sun relative to vertical at a particular time of day and location on the Earth's surface. The zenith angle is 0° when the Sun is directly overhead. At sunrise and sunset the zenith angle is near 90° . Local noon is defined as the time of day when the zenith angle is at a minimum.

At local noon on September 23 and March 21 (the equinoxes) the Sun is directly overhead at the equator. At noon on these two days the zenith angle at the equator is 0° . At noon on December 21 the zenith angle is 0° at the Tropic of Capricorn. Similarly, at noon on June 21 the zenith angle is 0°

on the Tropic of Cancer. Outside of the tropics (bounded by the Tropic of Cancer and the Tropic of Capricorn) the noon zenith angle can never be 0° . The noon time zenith angle must always be greater than 0° in the mid and polar latitudes.

The zenith angles for Los Angeles, California throughout the day on August 26, 2020 is shown in Figure 26 and Table 1. The Latitude for Los Angeles is N 34 degrees. On this particular day sunrise occurred at 05:23 and sunset occurred at 18:26 PDT. At local noon on this day the zenith angle for Los Angeles was 24.0 degrees.

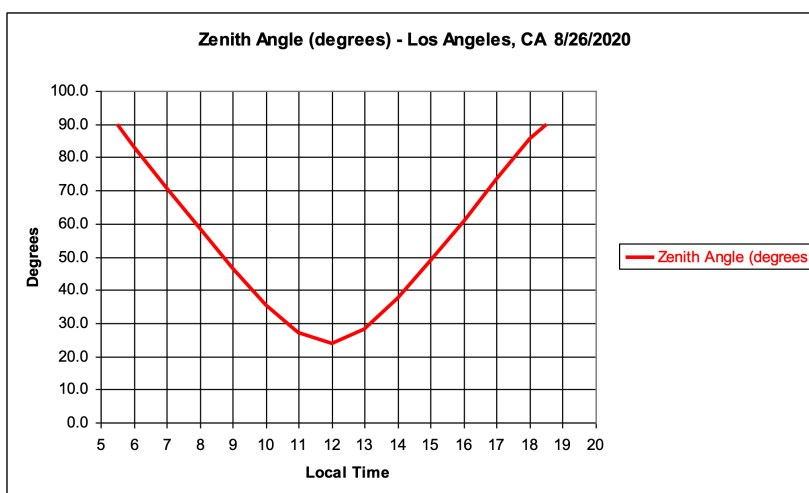


Figure 26 Typical zenith angle for Los Angeles, California (source: author)

Local Time (hour)	Zenith Angle (degrees)
5.5	90.0
6	83.1
7	70.8
8	58.5
9	46.5
10	35.5
11	27.1
12	24.0
13	28.3
14	37.4
15	48.7
16	60.8
17	73.2
18	85.4
18.5	90.0

Table 1 Zenith angles for Los Angeles, CA on August 26, 2020 (source: author)

The current sunspot number ($R = \text{SSN}$) can be found by clicking on “Solar Parameters” under the “Current Conditions” tab of the www.skywave-radio.org website. The current zenith angle cosine ($\cos Z$) is found by clicking on “Solar Position Calculator” under the Tools tab of the same website.

16.4.2 Seasonal Variations In Critical Frequencies

Seasonal changes in critical frequencies are due primarily to:

- Seasonal changes in zenith angles, and
- Seasonal changes in the Earth’s upper atmosphere.

Noon time zenith angles are always less in summer when the Sun is more overhead. We would thus expect critical frequencies to be higher in summer than in the winter. And they are for the E and F1 zones, but not so for the F2 region. During solar maximum F2 critical frequencies are substantially higher in winter than in summer, as illustrated in Figure 27, despite the fact that in winter the Sun is low in the sky. This is known as the seasonal anomaly.

As expected, E region critical frequencies are slightly higher in summer during both solar maximum and minimum. F1 critical frequencies are also higher in the summer during solar minimum. However, during solar maximum the F1 region is present during the summer but disappears in winter.

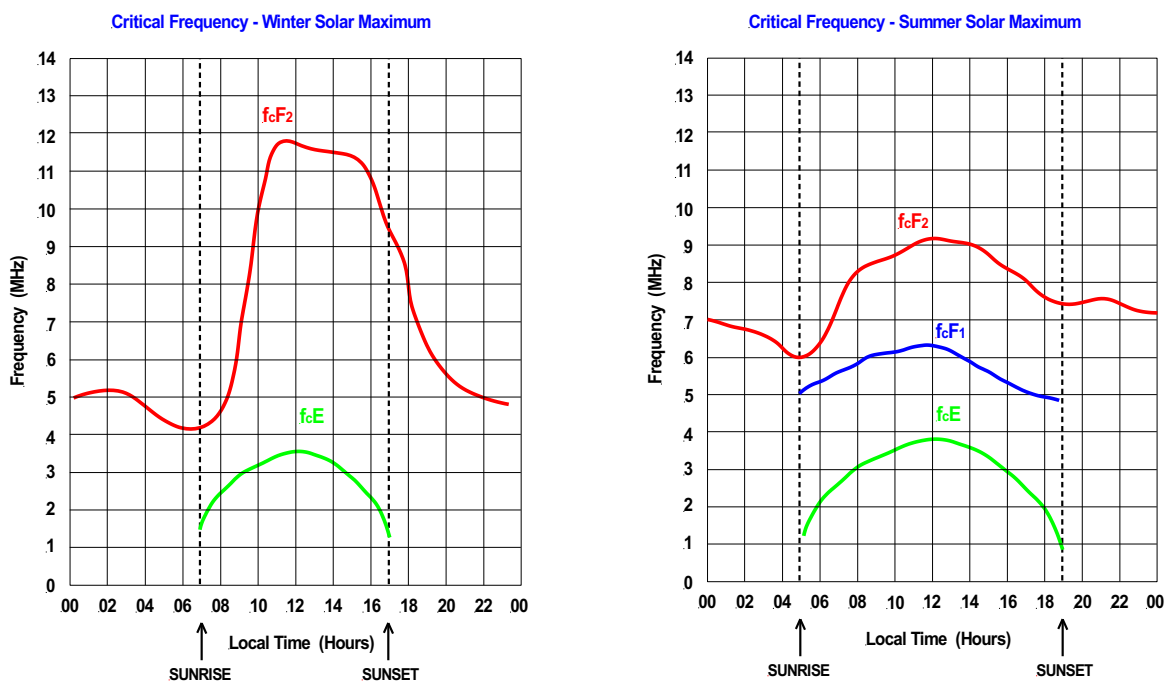


Figure 27 Winter and summer critical frequencies during solar maximum (source: author)

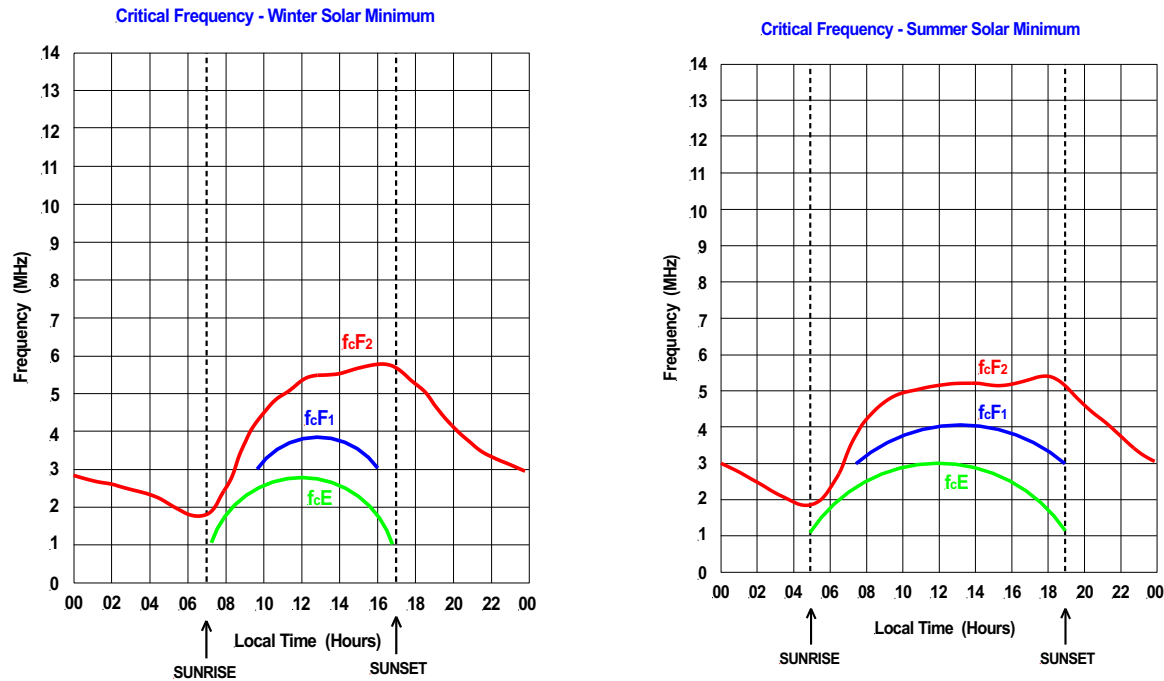
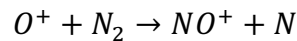


Figure 28 Winter and summer critical frequencies during solar minimum (source: author)

All critical frequencies are lower during solar minimum as illustrated in Figure 28. Low activity on the Sun means lower levels of EUV radiation available to ionize Earth's upper atmosphere. Consequently, critical frequencies are lower during solar minimum. In addition, F2 critical frequencies tend to peak in the late afternoon instead of around noon time (Figure 28). This is not what would be expected, but it is what happens. The F1 region appears in both the winter and summer during solar minimum.

Seasonal variations in F2 critical frequencies can be explained in part by changes in upper atmosphere chemical reaction rates plus changes in the ratios of major atmospheric species.

Reaction rates are generally temperature sensitive. For example, the first step in the dissociative recombination of atomic oxygen ions O^+ is



This reaction varies considerably with the temperature of neutral nitrogen N_2 . The reaction rate increases by a factor of 16 for a times 4 change in temperature. Changes in reaction rates contribute to both the F2 seasonal anomaly and persistence of the F region at night. During summer the higher temperature of N_2 increases the rate of dissociative recombination resulting in lower electron concentrations and lower F2 critical frequencies than in the winter. At night cooler

temperatures slow down the recombination process causing the F region to remain at least partially ionized.

Electron production rates in the F2 region depends on the concentration of atomic oxygen O while the recombination rate is controlled by concentrations of N₂ and O₂. An increase in atomic oxygen relative to molecular nitrogen and oxygen increases electron density. Thus, the ratio of atomic oxygen to molecular oxygen O/O₂ and atomic oxygen to molecular nitrogen O/N₂ is important. The ratio O/N₂ at an altitude of 300 km is about 6 in winter and around 2 in the summer, again resulting in lower electron densities and lower F2 critical frequencies in the summer compared to winter.

Summarizing, lower electron production rates in summer coupled with higher rates of recombination produce lower F2 critical frequencies in the summer than in winter.

16.4.3 Diurnal Variations In Critical Frequencies

Critical frequencies change throughout the day and night as shown in Figures 27 and 28. The change is driven by variations in ionization and recombination rates. Ionization of course only occurs during daylight hours whereas recombination is constantly occurring. It is important to note that daily variation in F2 critical frequencies follow a general trend but do not necessarily repeat from one day to the next, making predictions of F2 performance difficult.

At night the F1 and F2 regions combine forming a single F region. Ionization ceases at night, due to the lack of sunlight, while recombination continues. Consequently, electron density and F critical frequency decline throughout the night. F region critical frequency drops to its lowest level just before sunrise with f_cF around 2 – 3 MHz during solar minimum and 4 – 6 MHz during solar maximum.

Ionization resumes at sunrise causing the F region to split into two layers, the F1 layer and the F2 layer. The exception being in winter during solar maximum when the F1 layer does not form.

F2 critical frequency quickly increases following sunrise until around 10 AM to Noon when it plateaus as electron production and recombination rates reach equilibrium. In the winter, during solar maximum, the F2 region reaches its highest critical frequency around noon with critical frequencies typically from 9 – 12 MHz. It then declines in the late afternoon and throughout the evening as electron production decreases and finally stops. During solar minimum F2 critical frequency peaks around noon, levels off or slightly declines, and then peaks again at a higher frequency of around 5 – 6 MHz in the late afternoon, as illustrated in Figures 27 and 28.

During the day the F1 and E critical frequencies behave similar to Chapman layers. The F1 and E critical frequencies both increase rapidly following sunrise, peak at local noon, and decline in the afternoon. At night, the F1 region merges with the F2 region forming a single F layer. The E region does not completely disappear at night. At night $f_cE \sim 0.6$ MHz, a value which is too low to have any significant effect on HF communications. Thus, for practical purposes we assume that the E region also disappears at night.

Solar EUV radiation determines the degree of ionization during the day in Earth's ionosphere and thus daytime critical frequency levels. EUV radiation is constantly changing as the number and size of plagues, coronal loops and other disturbance on the Sun change. A measure of the radiation arriving from the Sun is provided by the Solar Flux Index (SFI). Solar flux is background solar radio noise caused by random collisions of electrons with heavier particles in the Sun's chromosphere and lower corona. The radio noise is measured daily by the Penticton Radio Observatory in British Columbia, Canada at a frequency of 2,800 MHz (10.7 cm wavelength). Solar Flux Index correlates well with measured levels of solar X-ray, Extreme Ultra Violate (EUV) radiation, and sunspot numbers as illustrated in Figure 29. SFI numbers vary from below 50 during solar minimum to above 300 at the peak of a solar cycle. A higher SFI number means a higher F2 critical frequency and better HF communications, particularly on the upper frequency bands of 20 through 10 meters. Current solar flux index is obtained by clicking on "Space Weather Conditions" under the "Current Conditions" tab at www.skywave-radio.org.

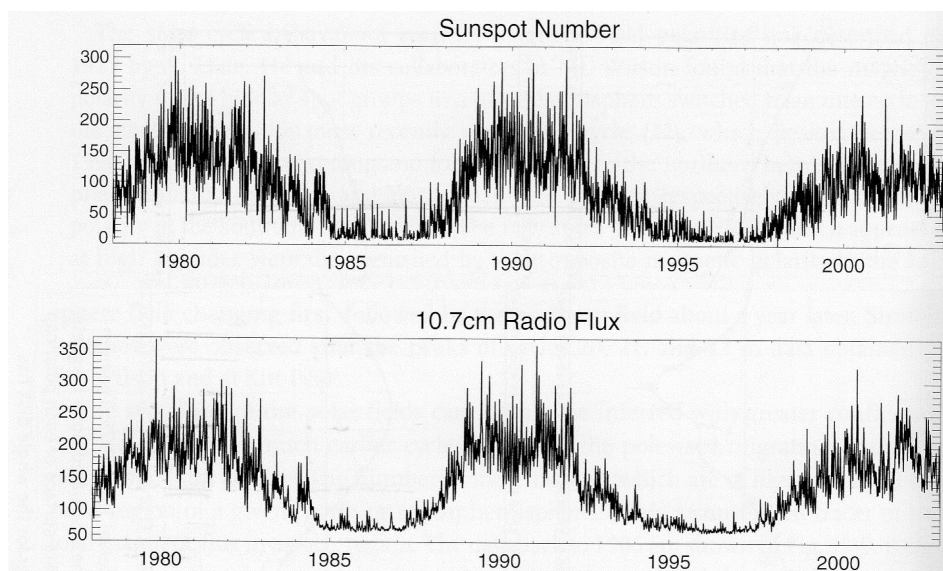


Figure 29 Radio flux vs Sunspot number (credit: G. deToma)

Critical frequencies are easily altered during the day and night by thermospheric winds which disrupt the wispy ionosphere continuously blowing it around.

The ionosphere is heated by excess photon energy above that necessary for ionizing neutral atoms and molecules. When a photon is absorbed by a neutral atom or molecule, energy in excess of that needed for ionization is transformed into the kinetic energy of the escaping electron as it speeds away from its parent atom or molecule. The higher the kinetic energy the greater the energy released in the form of heat when the electron collides with an atom or molecule. Because of this heating the ionosphere is hotter than the surrounding neutral atmosphere affecting the vertical distribution of plasma in the ionosphere's F2 region.

During ionospheric storms solar wind particles (electrons, protons, and some alpha particles) stream down into the high latitude auroral atmosphere. Collisions of these particles with neutral atoms and molecules change the chemical composition of the auroral ionosphere, heat the atmosphere, and change the circulation patterns of thermospheric wind. Heating plus changes in chemical composition accelerates the recombination of electrons with ions, decreasing electron densities in the auroral ionosphere. Convection currents carry the electron depleted auroral plasma down into mid latitudes causing F2 layer critical frequencies to drop by a factor of 2 or more. The drop in critical frequency impacts the higher HF bands more than lower frequencies. Radio frequencies from 20 through 10 meters are affected the most. These bands often disappear for a week or more.

16.4.4 F2 Critical Frequency Map

The issues causing fluctuations in critical frequencies from one day to the next are indeed complex. The best information on current critical frequency conditions is obtained from a world wide network of ionosondes. The critical frequency data from these ionosondes is integrated together by the Australian Government Bureau of Meteorology into a global F2 critical frequency map that is updated every 15 minutes. A typical map is shown in Figure 30. The current map is available by clicking on “Critical Frequency” under the “Current Conditions” tab at www.skywave-radio.org.

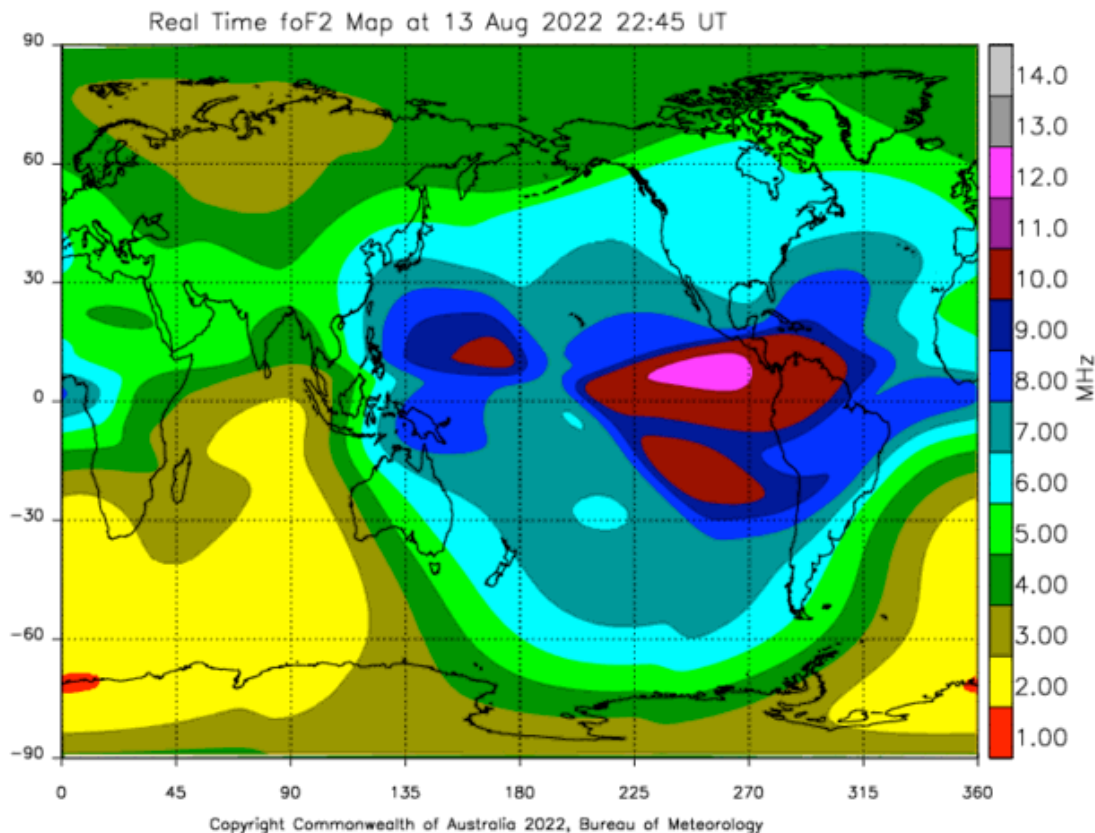


Figure 30 Critical Frequency Map (source: Australia Bureau of Meteorology)

The map shown in Figure 30 is for August 13, 2022 at 22:45 UT during the ascending phase of Solar Cycle 25. At this point in time the Sun was just emerging from sunspot minimum. Consequently, critical frequencies were close to sunspot minimum levels. The daytime F2 critical frequency for the United States was only 6 MHz. Consistent with solar minimum conditions, critical frequencies peaked in the late afternoon and early evening. Off the east coast of the United States critical frequency peaked around 7 MHz at 7 PM local time while it had been closer to 6 MHz earlier in the day.

Figure 30 clearly shows the winter anomaly. August is winter time in the southern hemisphere. Due to the winter anomaly we would expect F2 critical frequencies to be higher in the southern hemisphere than in the northern hemisphere, and they were. In the southern hemisphere the 7 MHz critical frequency band stretched down almost to 60° south latitude. However, in the northern hemisphere the 7 MHz critical frequency band extended only a little above 30° north latitude. In addition, significant segments of the 5 and 6 MHz critical frequency bands extended beyond 60° latitude in the southern hemisphere. Not so in the northern hemisphere. In the northern hemisphere only small segments of the 5 and 6 MHz critical frequency bands extended beyond 60° latitude. Darkness in the southern hemisphere at the time this map was generated produced night time critical frequencies as low as 2 MHz while long hours of sunlight in the Arctic region maintained critical frequencies at 4 MHz, just below daylight levels.

The highest critical frequencies occur in the tropics, as is the case in Figure 30. Notice in Figure 30 that patches of high critical frequency levels occurred on both sides of the equator. This is a typical example of the equatorial anomaly.

References

Hunsucker R. D.; Hargreaves, J. K.; “The High-Latitude Ionosphere and its Effects on Radio Propagation”; Cambridge University Press 2003

Davies, Kenneth; “Ionospheric Radio”; Peter Peregrinus Ltd., 1990

McNamara, Leo F.; “The Ionosphere: Communications, Surveillance, and Direction Finding”; Krieger Publishing Company, 1991

Nichols, Eric P.; “Propagation and Radio Science”; The American Radio Relay League, Inc. 2015

Yeang, Chen-Pang; “Probing The Sky With Radio Waves”; The University of Chicago Press, 2013

Devoldere, John; “Low-Band DXing” fourth edition; ARRL, 2005

Levis, Curt A. ; Johnson, Joel T.; and Teixeira, Fernando L.; “Radiowave Propagation Physics and Applications”; John Wiley & Sons, Inc., 2010

Ahrens, C. Donald; “Essentials of Meteorology”; Wadsworth Publishing Company, 1998

UCAR Center for Science Education (UCAR SciEd); <https://scied.ucar.edu/learning-zone/atmosphere/>

Khazanov, George V.; “Space Weather Fundamentals”; CRC Press, 2016

Foukal, Peter; “Solar Astrophysics third edition”; Wiley-VCH Publishing Company, 2013

Ganushkina, N. Yu.; Liemohn, M. W.; Dubyagin. S.; “Current Systems in the Earth’s Magnetosphere”; AGU, March 8, 2018

Gallagher, Dr. D.L.; “The Earth’s Plasmasphere”; Space Plasma Physics, Marshall Space Flight Center, Huntsville, AL, September 05, 2018

Moore, T. E., Morwitz, J. L.; “Stellar Ablation of Planetary Atmospheres”; August 9, 2007

Yau, Andrew W.; Abe, Takumi; Peterson, W. K.; “The Polar Wind: recent Observations”; Department of Physics and Astronomy, University of Calgary

Carroll, Bradley W. and Ostlie, Dale A.; “An Introduction to Modern Astrophysics”; Addison-Wesley Publishing Company Inc., 1996

Goodman, John M.; "Space Weather & Telecommunications"; Springer Science+Business Media Inc. 2005

Cander, Ljiljana R.; "Ionospheric Space Weather"; Springer Nature Switzerland AG 2019

Moldwin, Mark; "An Introduction to Space Weather"; Cambridge University Press, 2008

Campbell, Wallace H.; "Introduction to Geomagnetic Fields"; Cambridge University Press, 2003

Golub, Leon and Pasachoff, Jay M.; "Nearest Star The Surprising Science of Our Sun second edition"; Cambridge University Press, 2014

Loff, Sarah: "Explorer and Early Satellites"; National Aeronautics and Space Administration, Aug 3, 2017

Minzner, R. A.; "The 1976 Standard Atmosphere Above 86 km Altitude" NASA Goddard Space Flight Center, 1976